https://doi.org/10.5194/egusphere-2026-1631
Preprint. Discussion started: 18 May 2026

Acceleration After 2020 of Decreasing Earth Albedo from DSCOVR-EPIC 2015-2025 Compared with CERES 2000 - 2025

Jay R. Herman[1] and Jerald R. Ziemke[2]

[1]Goddard Earth Sciences Technology and Research-2 (GESTAR-2) University of Maryland Baltimore County, Baltimore Maryland, USA

[2]1Goddard Earth Sciences Technology and Research II (GESTAR-2) Morgan State University, Baltimore, Maryland, USA

https://doi.org/10.5194/egusphere-2026-1631
Preprint. Discussion started: 18 May 2026

29 Abstract

30 The 10-year Earth albedo time series, its seasonal and wavelength dependence (10
31 wavelengths from 317.5 to 779.5 nm) of the illuminated Earth are estimated from radiance
32 measurements by the Earth Polychromatic Imaging Camera EPIC located in an orbit
33 around the Earth-Sun Lagrange-1 point L_1. The calibration of the EPIC channels, especially
34 443 nm to 780 nm has not changed during the 10 years of operation.The measurements
35 were made at a backscattered observing phase angle ranging from 2^O to 12^O. The maximum
36 albedo occurs at 340 nm, ranging from 0.33 in June to 0.38 in December. For shorter
37 wavelengths, 325 and 317.3 nm, the albedo decreases sharply because of ozone
38 absorption. For wavelengths longer than 340 nm (388, 443, and 551 nm) the albedo
39 decreases gradually until about 680 nm where reflectivity from vegetation increases (680
40 and 779.5 nm). The maximum albedo occurs in December when the illuminated Antarctic
41 ice sheet is observed. The EPIC solar flux weighted annual mean albedo in 2016 is
42 estimated to be 0.298 (317.5 to 779.5 nm) and 0.293 in 2025, (-1.7% change) compared to
43 the Clouds and the Earth's Radiant Energy System (CERES) 2016 values of 0.289 and 0.288
44 in 2026 (-1.3% change) after a small recovery in 2024 for the spectral range 300 to 5000 nm.
45 The long-term change of CERES albedo R_{AC} (2000 – 2026) is 1.6% over 26 years, The CERES
46 albedo shows an accelerating decline after 2022, R_{AC} (2022 – 2024) = 0.2 % yr^{-1} compared to
47 R_{AC} (2000 - 2020) -0.07 % yr^{-1}. EPIC observes similar rates of albedo decline, R_{AE} (2016-
48 2019.5) = -0.12 % yr^{-1} and R_{AE} (2020.3-2025.8) = 0.23 % yr^{-1} validating the occurrence of an
49 increased rate of albedo decline after 2022. After 2024 CERES sees a small albedo
50 recovery that is larger than seen by EPIC. Both EPIC and CERES albedo data suggest that
51 the accelerating reduced Earth reflection of sunlight back to space is enhancing global
52 warming.

53

54

55 Plain Language summary

56 The brightness of the reflected sunlight has been estimated by two independent satellite
57 observations, EPIC (Earth Polychromatic Imaging Camera) in an orbit around the Earth-Sun
58 gravitational balance point, 1.5 million km from Earth, and CERES (Clouds and the Earth's
59 Radiant Energy System). Both measurements show that the amount of reflected light from
60 the Earth has decreased since 2016 and with a faster rate of decrease since 2022. The
61 decreased Earth reflectivity enhances the effect of global warming from increased
62 amounts of carbon dioxide and methane in the atmosphere.

https://doi.org/10.5194/egusphere-2026-1631
Preprint. Discussion started: 18 May 2026

1.0 Introduction

The short wavelength, UV, Visible, and Near-IR, reflectance (albedo) of the Earth is fundamental to our understanding of the energy balance between solar input and reflected energy back to space. Early satellite instruments such as the Earth Radiation Budget Experiment (ERBE) and ScaRaB (Scanner for Radiation Budget) **)** provided global, angularly resolved observations of outgoing shortwave radiation, from which top-of-atmosphere (TOA) albedo could be derived using angular distribution models (Barkstrom, 1984; Taylor & Stowe, 1984). These data sets produced the first consistent climatology of planetary albedo and its partitioning among clouds, atmosphere, and surface (Harrison et al., 1990). They established that on average roughly one-third of incoming solar radiation is reflected back to space (Stephens et al., 2015). These low Earth orbiting (Wang et al., 2015; Goode et al., 2001; Lucht et al., 2000; Tosco et al., 2025) demonstrated that clouds, ice and snow cover, and ocean–land surface contrasts are the dominant contributors to planetary reflectance. Later satellite instruments, including the Clouds and the Earth's Radiant Energy System (CERES), improved radiometric accuracy, angular sampling, and long-term stability, making it possible to detect subtle interannual variations in albedo associated with large-scale modes of climate variability (Wielicki et al., 1996; Loeb et al., 2009). Starting in 2020, the change from high-sulfur "bunker" fuel to low-sulfur alternatives appears to have a side effect of accelerating global warming (Gettelman et al., 2024; Yuan et al., 2022; Mace et al., 2026) because lack of sulfate aerosols from ship emissions no longer tend to brighten clouds (bright ship tracks). Model studies suggest that the sulfate aerosol reduction is not enough to explain the observed warming (Gettelman et al., 2024).

Multispectral imagers such as the Advanced Very High-Resolution Radiometer (AVHRR**)** enabled global mapping of surface albedo at much finer spatial scales. Retrieval algorithms exploiting multi-angular and multi-band reflectance were applied to more than four decades of AVHRR Global Area Coverage (GAC) data, producing consistent global surface albedo products suitable for climate studies and land–atmosphere coupling research (Csiszar and Gutman, 1999; Liu et al., 2009). These records document both the strong spatial gradients in albedo across deserts, vegetated regions, snow and ice, and the temporal evolution associated with land-use change, snow cover variability, and cryospheric retreat (Schaaf et al., 2002; He et al., 2014).

Earth albedo measurements were also determined piecemeal from Earthshine data (Stephens et al., 2015; Goode et al., 2001; 2021). Photometric measurements are made of

https://doi.org/10.5194/egusphere-2026-1631
Preprint. Discussion started: 18 May 2026

sunlight reflected from Earth to the dark side of the Moon and back to ground-based telescopes. In this technique, the ratio of the lunar dark-side radiance (illuminated by Earth) to the bright-side radiance (illuminated directly by the Sun) is used to infer Earth's disk-integrated reflectance (Goode et al., 2001). A systematic earthshine program operated from Big Bear Solar Observatory has provided a multi-decadal record of terrestrial albedo variations, demonstrating the feasibility of monitoring global-mean albedo from the ground and offering an independent check on satellite-derived trends (Pallé et al., 2004; Qiu et al., 2023). The estimated trends showed a decline in albedo since 1990 consistent with satellite measurements.

Satellite missions, particularly NASA's CERES (Clouds and the Earth's Radiant Energy System), launched in 1999, provide the most comprehensive long-term record of Earth's reflected solar radiation. CERES data confirms the Earthshine-derived albedo trends and remains essential for quantifying Earth's energy imbalance, an imbalance driven by the difference between absorbed solar radiation and outgoing longwave radiation.

This study examines a unique set of albedo measurements that was obtained from the DSCOVR satellite viewing almost the entire illuminated sun-facing Earth and is a follow-on to the DSCOVR-EPIC study by Yang et al. (2018) and Penttilä et al. (2022). Launched in 2015, the Deep Space Climate Observatory (DSCOVR) satellite was placed at the Earth-Sun gravitational balance Lagrange point L_1, approximately 1.5 million kilometers from Earth, to continuously observe the full sunlit disk of our planet. Its Earth Polychromatic Imaging Camera (EPIC) captures high-resolution images in 10 narrow-band spectral channels (Table 1 and Fig.1) spanning ultraviolet to near-infrared wavelengths (317.5–779.5 nm), supporting studies of ozone, aerosols, clouds, vegetation, and surface UV radiation. Table 1 contains the wavelength, the uncertainty of the center of each band, full width half maximum (FWHM), and the conversion coefficient for the measured counts per second to Lambert equivalent albedo (Marshak, et al., 2018). In addition, the accurate radiometric calibration of EPIC enables estimates of albedo for phase angles near the backscatter direction, approximately 168^{o} to 178^{o}. The calibration of the EPIC channels, especially 443 nm to 780 nm has not changed during the 10 years of operation (Cede et al., 2025).EPIC measures radiance in counts/second from each CCD pixel in each wavelength channel and converts it into albedo (Marshak et al., 2018) that can be applied to images of the Earth, Moon, and Jupiter (Herman and Blank, 2026). Other planets (e.g., Mars) occupy too few pixels for successful EPIC measurements.

https://doi.org/10.5194/egusphere-2026-1631
Preprint. Discussion started: 18 May 2026

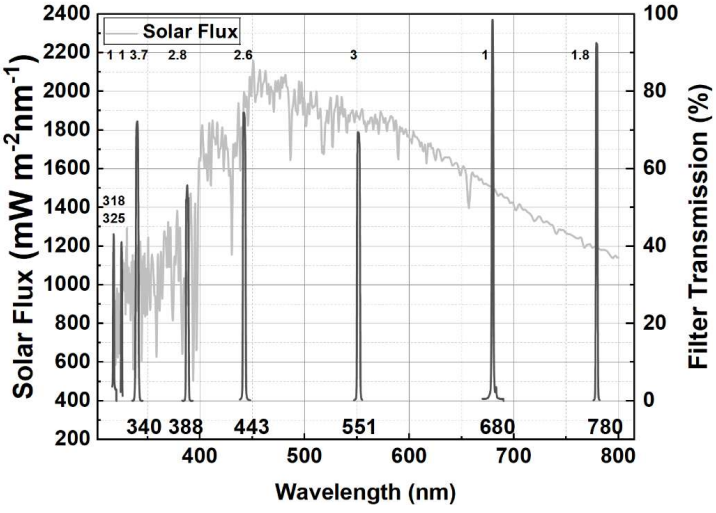

Fig. 01 EPIC filter transmission (%) right axis and Solar flux mW m^{-2} nm^{-1} grey curve left axis. Numbers at the top are the FWHM of each EPIC filter (Table 1).

We will show the narrow band wavelength dependence of the Earth's albedo for 317.5, 325, 340, 388, 443, 551, 680, and 780 nm. Two other wavelengths are available, 688 and 764 nm that are both absorbed by O_2 in the atmosphere and will not be used to estimate the total EPIC observed Earth Albedo. The 8-filter bands and their FWHM (Full Width Half Maximum) are shown in Fig. 1 superimposed on a typical solar spectrum at 1 AU from the sun.

Secular long-term albedo trends will be shown for the solar flux weighted average of 8 wavelength channels and are compared with trends derived from publicly available CERES data sets (Su et al., 2018; Wu et al., 2023; Goessling et al., 2025), which can be found at https://ceres-tool.larc.nasa.gov/ord-tool/jsp/EBAFTOA421Selection.jsp.). Based on the work of Su et al., 2018, "The global monthly mean daytime SW fluxes from EPIC agree with those from CERES to within 2%" when corrected for a small missing portion of the Earth's surface not seen in each EPIC image (3 to 8%) depending on EPIC's orbital position.

The basic EPIC data consists of measured counts per second in each of the 10-wavelength images of the sunlit Earth obtained every 1 to 2 hours as the Earth rotates at 15° per hour. The coverage is from sunrise to sunset in each wavelength image. Combining each day's set of images gives the entire radiation reflected back to space for 24 hours in counts per second. The result is a time series (Fig.2) for each wavelength channel. The counts per second are converted to albedo using the multiplicative conversion factors K_λ in Table 1.

https://doi.org/10.5194/egusphere-2026-1631
Preprint. Discussion started: 18 May 2026

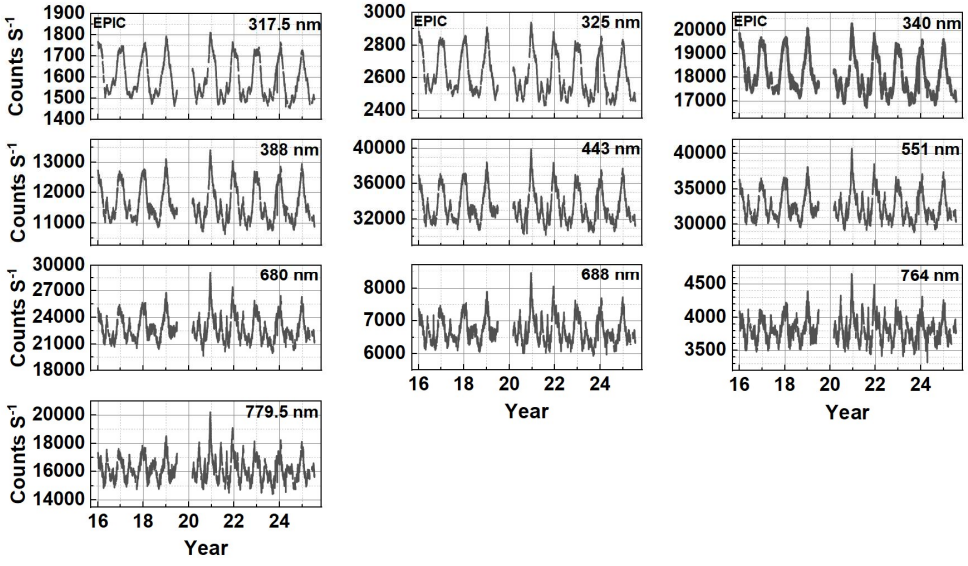

Fig. 02 Global average daily time series in counts per second for each of the 10 wavelength channels for the period 2015.5-2025.6. There is missing data starting from 2019.5 to 2020.3. Only days with complete global coverage were used.

2.0 Discussion

EPIC is built around a 30-cm f/9.6 Cassegrain telescope with a 2.855-meter focal length, imaging onto a 2048 × 2048-pixel hafnium-coated UV sensitive silicon CCD detector. This configuration enables EPIC to nearly fill its 0.62° field of view with the Earth's disk when closest to the Earth. Full disk images are acquired every 60 to 100 minutes, allowing for dynamic monitoring of Earth's atmosphere and surface. The 10 filter wavelength channels, their FWHM albedo conversion coefficients, and exposure times are shown in Table 1.

To ensure scientific accuracy, EPIC has undergone extensive in-flight calibration, including flat-fielding to correct pixel-to-pixel sensitivity variations and geometric stray light correction (Cede et al., 2021). Stray light, caused by internal reflections and scattering within the optical system, can significantly distort radiometric measurements, especially in the ultraviolet channels critical for ozone retrieval (Cede et al., 2021). During the 10-year lifetime of EPIC, wavelength-dependent correction algorithms have been developed that model and subtract stray light contributions based on the detector response characteristics. These corrections are essential for accurate retrievals of total column ozone (Herman et al., 2018; 2025) and other atmospheric constituents, particularly in the UV range where signal contamination is most pronounced.

https://doi.org/10.5194/egusphere-2026-1631
Preprint. Discussion started: 18 May 2026

Table 1 Wavelengths, FWHM, Albedo conversion coefficients, exposure time

Wavelength nm	FWHM nm	K_λ(1 AU) Sec counts^{-1}	Exposure ms
317.5 ± 0.1	1	1.216×10^{-4}	653±0.12
325.0 ± 0.1	1	1.111×10^{-4}	442±0.11
340.0 ± 0.3	3.7	1.970×10^{-5}	65±0.16
388.0 ± 0.3	2.6	2.685×10^{-5}	86±0.16
443.0 ± 1.0	2.6	8.340×10^{-6}	28±0.06
551.0 ± 1.0	3	6.660×10^{-6}	22±0.04
680.0 ± 0.2	1.6	9.300×10^{-6}	32±0.04
687.75 ± 0.2	0.84	2.020×10^{-5}	75±0.03
764.0 ± 0.2	1	2.360×10^{-5}	102±0.04
779.5 ± 0.3	1.8	1.435×10^{-5}	46±0.14

EPIC multiplicative albedo calibration coefficients K_λ (Table 1) are used to convert counts per second into top-of-atmosphere Lambertian albedo $A_\lambda = \pi I_\lambda / S_\lambda$ where I_λ = the outgoing radiance at the top of the atmosphere and S_λ is the incoming corresponding solar flux. The factor π converts I_λ / S_λ to the equivalent Lambertian albedo A_λ. The quantity I_λ is a function of the observing angle, which in EPIC's 2024 case is close to a 170^O backscatter angle.

An example of such a calculation is shown in Fig.3 for 443 nm on 15 March 2024 at 11:52.27 GMT. The full Earth has relatively low albedo because of the presence of low-reflectivity oceans covering most of the surface (71%), when under almost cloud-free conditions. This particular image is centered over Africa at approximately 2^{O}W longitude (Fig.4). In this image, Africa is mostly cloud-free except for a circle of clouds just below the equator having an albedo of about 0.9 and low clouds with an albedo of about 0.35. The clear sky 443 nm background has an albedo (blue) of about 0.2. The backscatter phase angle is approximately 170^O or observing phase angle of 10^O.

https://doi.org/10.5194/egusphere-2026-1631
Preprint. Discussion started: 18 May 2026

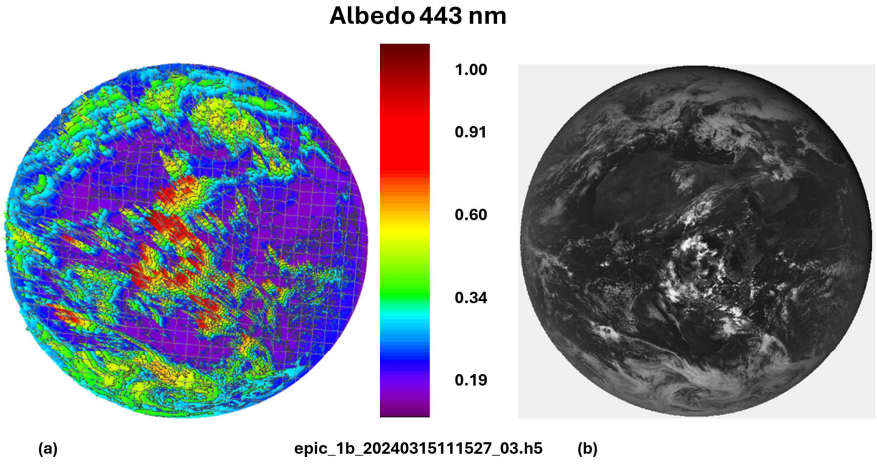

Figure 03 (a) Estimated albedo from the 443 nm image (b) in counts sec^{-1} centered over Africa at 11:15:27 GMT as shown in the color image in Fig. 4. The EPIC hdf5 counts sec^{-1} data file is epic_1b_20240315111527_03.h5

193

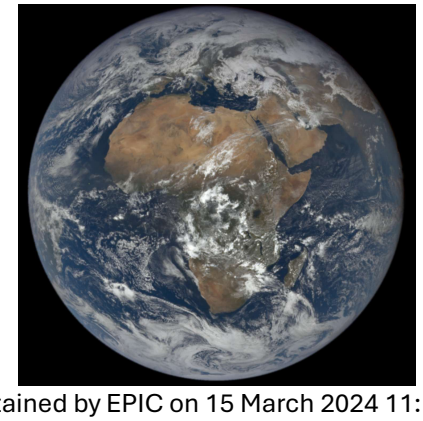

Fig 04 Full color image obtained by EPIC on 15 March 2024 11:52.27 GMT

194

195

196

197

198

199

200

https://doi.org/10.5194/egusphere-2026-1631
Preprint. Discussion started: 18 May 2026

2.1 Lunar Albedo

A similar set of images can be obtained for the Earth's moon at 443 nm showing the albedo derived from conversion coefficient for 443 nm in Table 1.

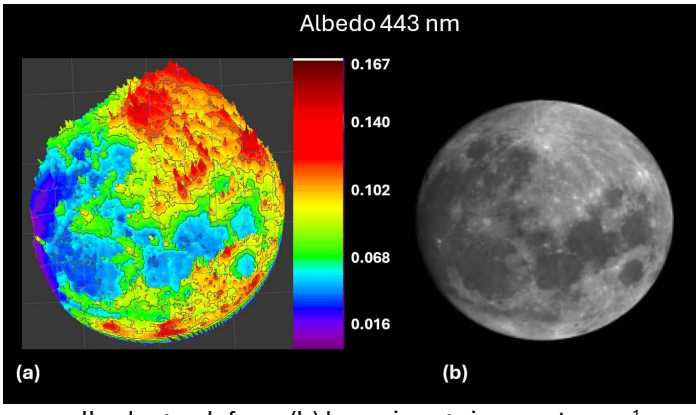

Fig. 05 (a) 3-D Lunar albedo graph from (b) lunar image in counts sec^{-1}

The albedo of the moon is almost invariant based on the extensive ROLO (RObotic Lunar Observatory) observations for a given observing phase angle (Keiffer and Stone, 2005), which in this case (Fig. 5) is approximately 10^{O}. The ROLO data encompasses a wide range of phase angles from 1.55^{O} to 97^{O}, where the 1.55^{O} phase angle corresponds to the almost full moon in opposition as seen from the Earth. EPIC lunar calibration is always performed at times when the full moon is observed from the Earth with its familiar face always pointing to the Earth with only a small nutation variation during the year. EPIC observes the almost full moon (Fig. 5) when it is slightly displaced from the Earth by a few degrees (always less than 4^{O} as seen from EPIC) but far enough away from the Earth (about 2^{O} or 4 Earth diameters) to avoid Earth stray light entering the EPIC telescope. These lunar observations are used to ensure that the EPIC calibration at each wavelength remains invariant and to correct for pixel-to-pixel variations (flat-fielding).

A ROLO data comparison (Jones et al., 2013) with EPIC whole illuminated average disk albedo at a phase angle of approximately 10^{O} obtained on 21 May 2024 19:32:50 GMT is shown in Fig. 6. Similar EPIC comparisons on other full moon days (as observed from the Earth) are almost identical.

https://doi.org/10.5194/egusphere-2026-1631
Preprint. Discussion started: 18 May 2026

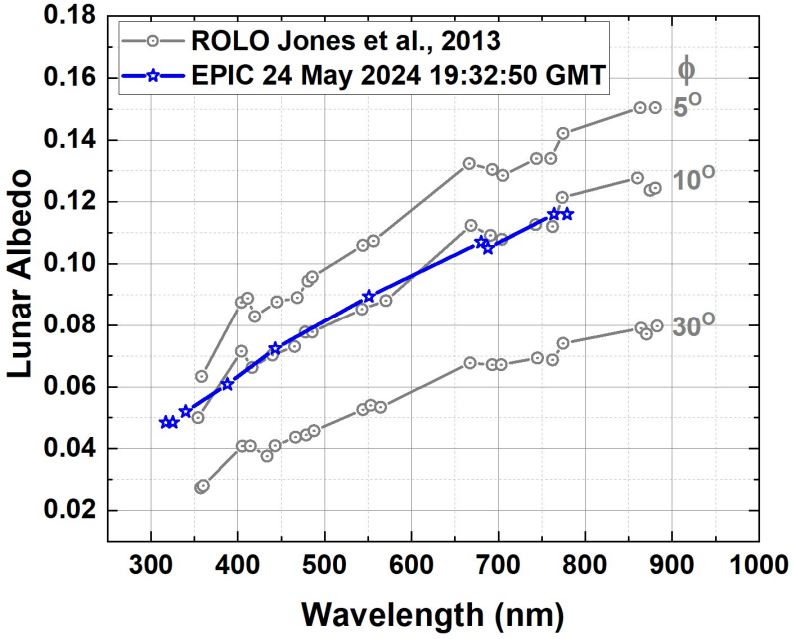

Fig. 06 A comparison of EPIC estimated whole disk average lunar albedo (stars) at 10 wavelengths 21 May 2024 19:32:50 GMT with ROLO whole disk average albedo at $\phi = 5^{O}$, 10^{O} and 30^{O} phase angles (Jones et al., 2013)

Figure 5 shows that there is a wide range, 0.02 to 0.16, of albedos as a function of position on the lunar surface from the so-called highlands and mare. The comparison of the "full moon" surface average albedo with ROLO data as a function of wavelength (Fig. 6) suggests that the EPIC calibration for conversion of counts per second to albedo is accurate. A similar comparison of EPIC albedo data for Jupiter (Herman and Blank, 2026) with spectroscopic measurements (Karkoschka et al., 1994; 1998) shows similar agreement.

2.2 Earth Albedo Wavelength Dependence

Extensive measurements of Earth albedo have been made by EPIC for the past 10 years at a rate of once per hour in Northern Hemisphere (NH) summer (April to August) and once every 2 hours (September to March). The cadence is dictated by the number of hours that the receiving antenna at Wallops Island Virginia is in view of the DSCOVR spacecraft at L_1.

The Earth is observed every 1 to 2 hours while rotating at 15^{O} per hour with a full rotation every 24 hours. Unlike the invariant Moon, the Earth has extensive weather patterns that

https://doi.org/10.5194/egusphere-2026-1631
Preprint. Discussion started: 18 May 2026

change day to day (cloud cover), a molecular and aerosol atmosphere with Rayleigh and Mie scattering, and seasonal changes in surface reflectivity (vegetation and snow/ice).

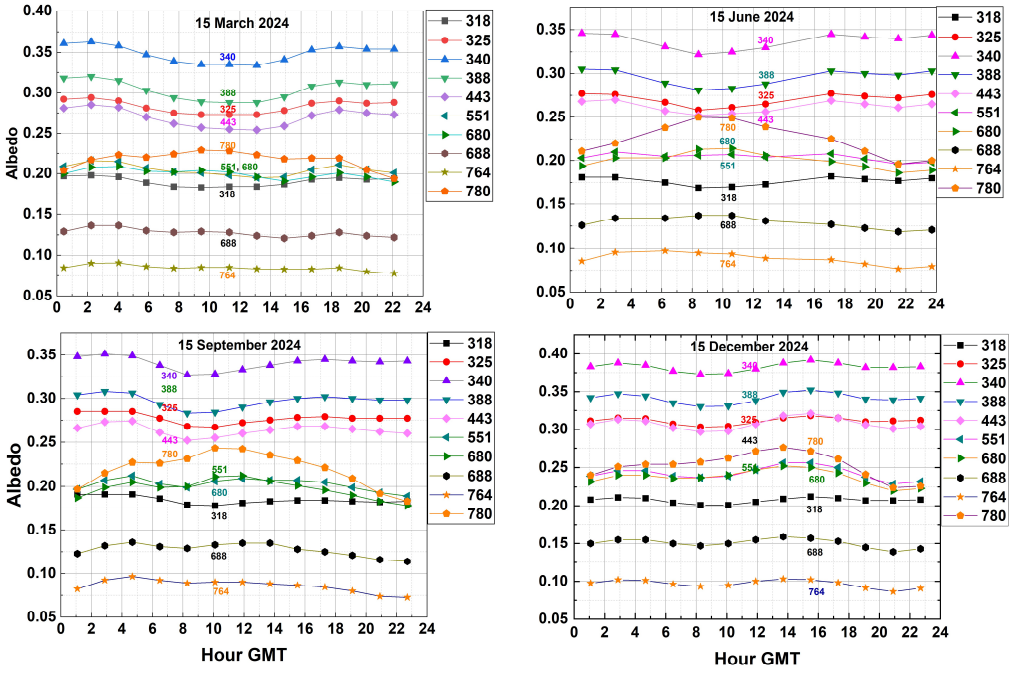

Fig. 07 The hourly GMT variation in whole illuminated Earth albedo for the middle of March, June, September, and December 2024. For 12 GMT the EPIC image longitude is centered over Greenwich, England. For 17 GMT the image longitude is centered over the US east coast (75^{O}W).

Of the 10 EPIC channels, two were selected to match part of the absorbing oxygen A- and B-bands used for estimation of cloud height and aerosol plume height (Yin et al., 2020; Xu et al., 2020). The albedo estimates for these channels, 687.75 ± 0.2 and 768 ± 0.2 nm are much lower (Fig. 7) than for surrounding non-O_2 absorbed wavelength channels. These are narrow band channels with the FWHM Δ = 0.84 and 1 nm for 687.75 and 768 nm, respectively.

As examples, the average illuminated Earth disk albedos are computed for each wavelength as a function of GMT (Earth's rotation) in Fig. 7. The hourly albedos show clear patterns with the UV 325 nm to blue (443 nm) channels having a minimum albedo for images centered near the morning GMT in March (11 GMT or 15^{O}E), June (8 GMT or 60^{O}E), September (8 GMT or 60^{O}E), and December (8 GMT or 60^{O}E). The 317.5 nm channel (labelled 318) has low albedo values caused by atmospheric ozone absorption. The visible

https://doi.org/10.5194/egusphere-2026-1631
Preprint. Discussion started: 18 May 2026

and near-infrared channels (551, 689 and 779.5 nm) mostly have a peak over the bright African surface (Fig. 4).

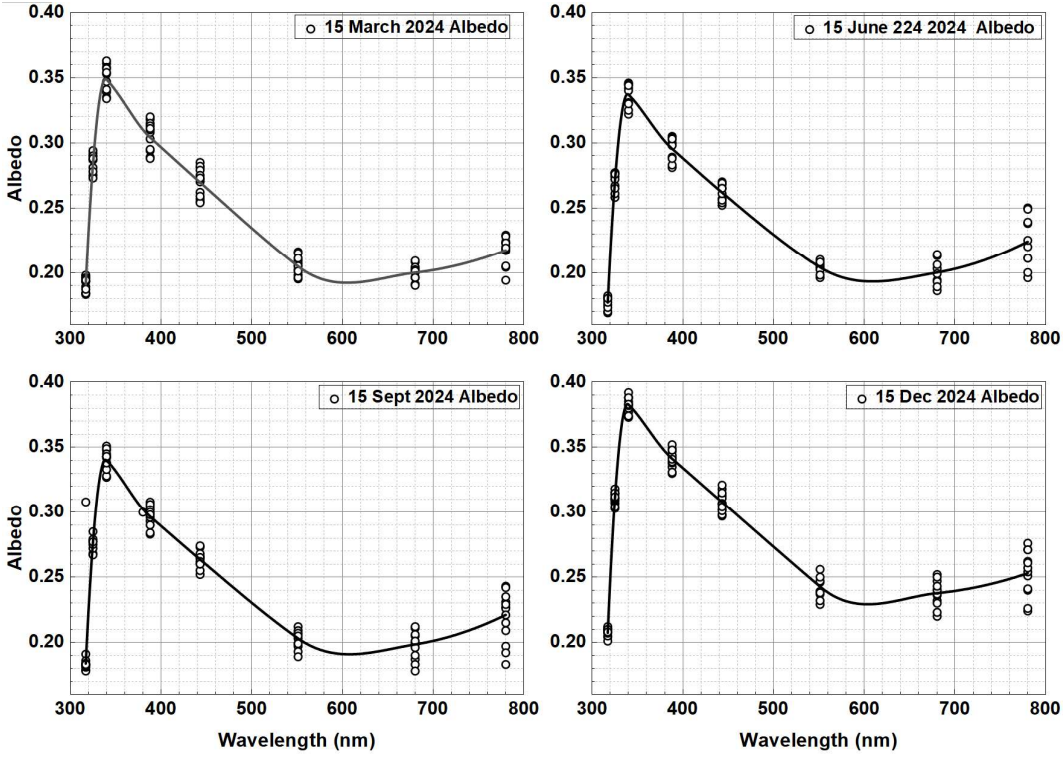

Fig. 08 Seasonal mid-month mean albedo with hourly spread (small circles) as the Earth rotates. The smooth curves are Akima spline-fits (Akiima, 1970)

The seasonal differences in albedo as a function of wavelength are shown in Figs. 7 and 8. Fig 7 shows the hourly variation for each wavelength on the specified day as the Earth rotates. The maximum albedo occurs in December (Fig. 9) when the Antarctic ice sheet is observed as the Earth's rotation axis tilts the SH 23.5^{O} toward the Sun and EPIC.

https://doi.org/10.5194/egusphere-2026-1631
Preprint. Discussion started: 18 May 2026

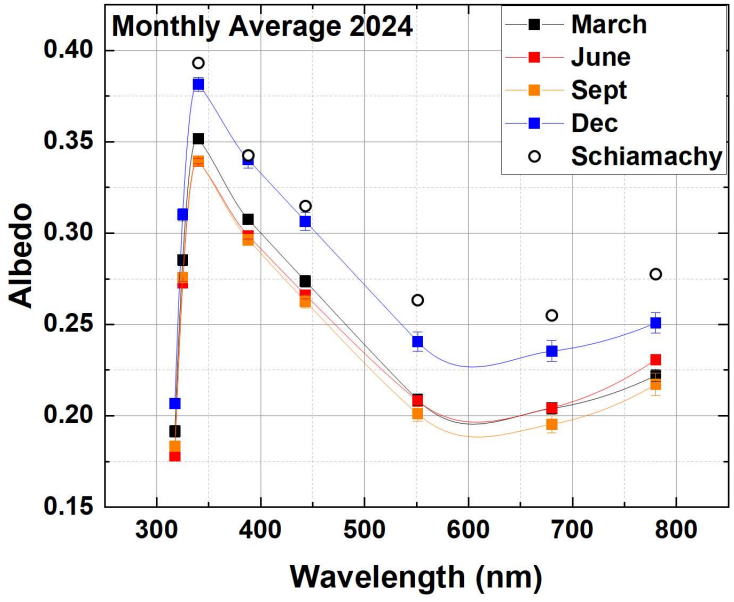

Fig. 09 The monthly average of the almost fully illuminated Earth disk for in March, June, September, and December 2024. The smooth curves are Akima spline-fits (Akima, 1970) to the 8 EPIC data points. The small circles are Sciamachy data from Stephens et al., 2015.

260

261 **2.3 Long-Term Albedo Trends**

262 CERES data (https://ceres-tool.larc.nasa.gov/ord-tool/jsp/EBAFTOA421Selection.jsp) were
263 obtained from a uniform monthly grid (Figs. 10a and 10b). The CERES average Earth albedo
264 Fig. 10c can be derived from the ratio of the outgoing all-sky top of the atmosphere flux (Fig.
265 10a) to the incoming solar flux (Fig. 10b). The long-term average (blue curve Fig. 10c and
266 10d) is a Lowess(f) fit to the ratio (Cleveland and Devlin, 1988). Here the fraction f = 0.2, or
267 5.2 years of CERES data.

268

https://doi.org/10.5194/egusphere-2026-1631
Preprint. Discussion started: 18 May 2026

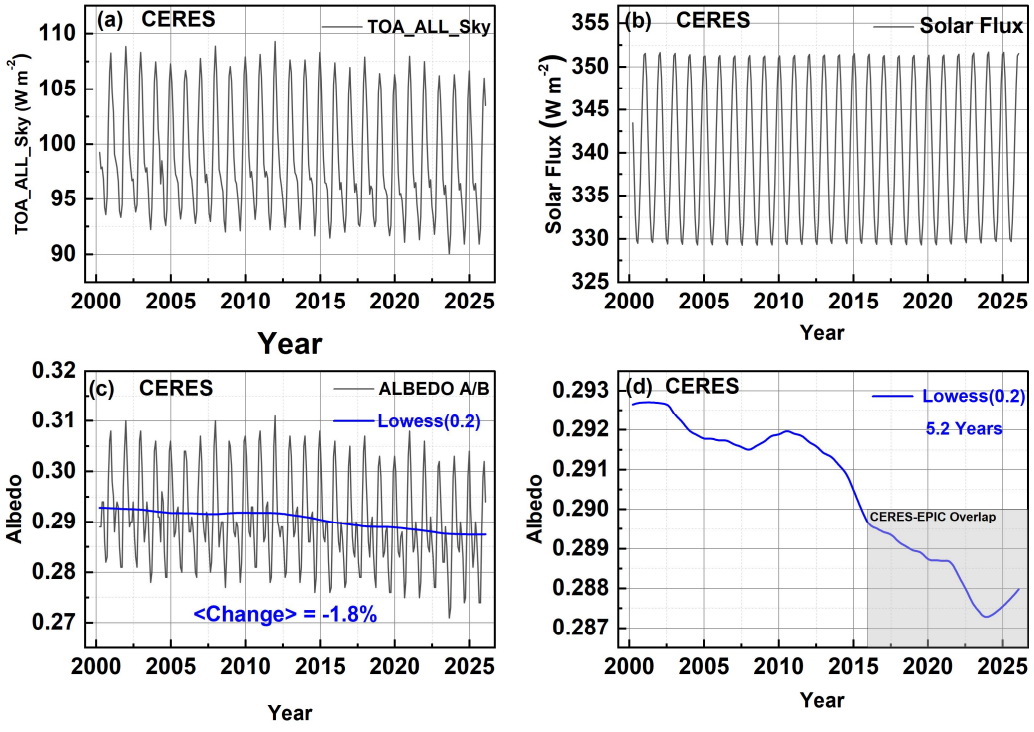

Fig. 10(A) CERES TOA outgoing all-sky short-wave flux(B) Incoming Solar Flux (C) CERES whole Earth albedo 15 August 2000 to October 2025 smoothed with a Lowess(0.2) blue line, (D) Lowess(0.2) on an expanded scale showing EPIC overlap starting in 2016. The grey box shows the overlap period with EPIC.

±

https://doi.org/10.5194/egusphere-2026-1631
Preprint. Discussion started: 18 May 2026

The decreasing CERES albedo over the past 25 years shown in Fig.11 suggests increasing positive feedback from global warming after 2020 from likely decreases in cloud cover and the decrease in polar ice sheets.

In order to compare CERES albedo trend estimates with those from EPIC, the time series in Fig. 10 is truncated to the range from 2016 to 2025 to match that from EPIC. The results from a linear fit to the truncated LOWESS (0.2) data are shown in Fig. 11 and Table 2.

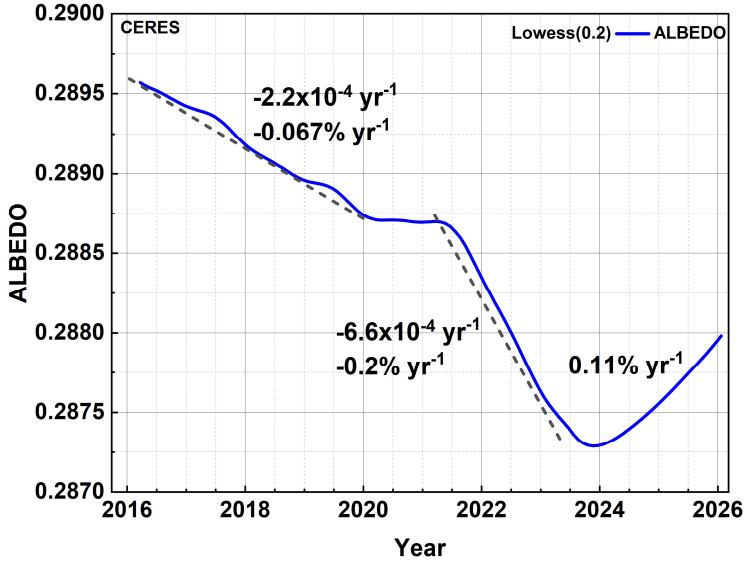

Fig. 11 Albedo trend estimates from CERES data 2016 – 2025. The dashed line is a linear fit to the Lowess(0.2) smoothed data from Fig. 10 displaced slightly to the left.

When weighted by the Solar flux (Fig. 1), the annual average EPIC albedo is 0.2986 in 2016 (Fig. 12) and decreases to 0.2873 in 2023.7, a decrease of 0.8% followed by a period of recovery after 2024.

https://doi.org/10.5194/egusphere-2026-1631
Preprint. Discussion started: 18 May 2026

283

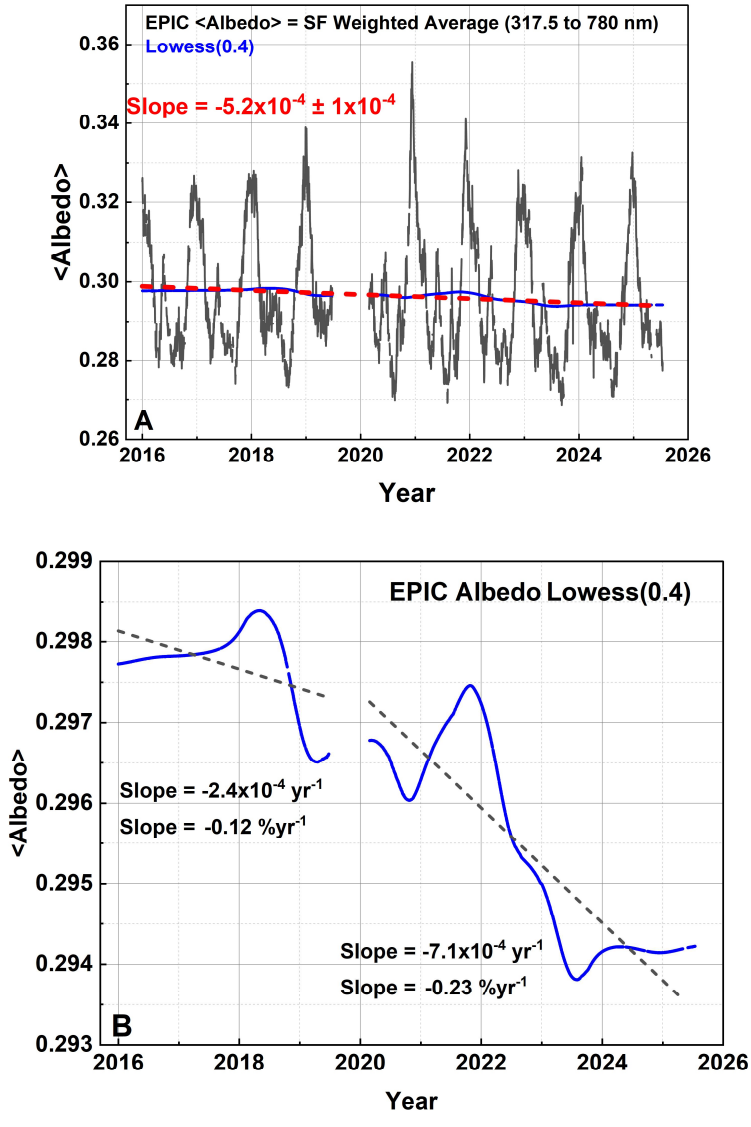

Fig. 12 A. EPIC solar flux weighted average albedo time series (317.5 to 780 nm). B. Lowess(0.4) and linear fit to the time series for the periods 2016 to 2019.5 and 2020.3 to 2025.5.

284

285 The time series in Fig. 12A and the individual time series in Fig. 2 have main frequency
286 components of 1 year, half a year, approximately ¼ year. The approximately ¼ year

https://doi.org/10.5194/egusphere-2026-1631
Preprint. Discussion started: 18 May 2026

287 component comes from the changing observing phase angle between the EPIC instrument
288 and the Earth-Sun line as part of DSCOVR's approximately six-month orbit about L_1.

289

Table 2 Trend estimates R in percent change per year

CERES	EPIC
R_C (2016-2020) = -0.07 % yr^{-1}	R_E (2016-2019.5) = -0.12% % yr^{-1}
R_C (2021-2024) = -0.2 % yr^{-1}	R_E (2020.3-2025.8) = -0.23 % yr^{-1}
R_C Total (2016-2026) = -1.3%	R_E Total (2016-2025.8) = -1.7%
R_C Total (2000-2026) = -1.6%	

290

291 The trend estimates for the percent change in albedo estimated from both CERES and EPIC
292 are similar in the 2020 to 2025 period showing an accelerated albedo decline relative to the
293 earlier 2016 to 2020 period (Table 2). CERES trend estimates in the 2016 to 2020 period are
294 smaller than those estimated from EPIC. The increased rate of decline in albedo after 2021
295 is present in both data sets suggesting that the CERES measured albedo decreases are not
296 caused by calibration drift.

297

298 **3.0 Summary**

299 Measurements of the short wavelength Lambertian albedo 317.5 to 779.5 nm behavior of
300 the whole illuminated Earth has been obtained from the DSCOVR-EPIC instrument. The
301 calibration of the EPIC channels, especially 443 nm to 780 nm has not changed during the
302 10 years of operation (Cede et al., 2025). The results are comparable to results from CERES
303 and Sciamachy. In 2016 CERES measured a global average albedo of 0.289 (300 – 5000 nm)
304 compared to the EPIC value of 0.298 (318 – 780 nm). The 2016-2026 CERES albedo
305 decline is -1.3%, while the EPIC decline is 1.7%. The long-term CERES and EPIC albedo
306 time series show an increased rate of decline after 2022 (-0.2% yr^{-1} for CERES and -0.23%
307 yr^{-1} for EPIC). The important point is that both independent data sets show an accelerated
308 albedo decline after 2022.

309 Comparison with ROLO ground-based lunar albedo measurements show that EPIC's
310 wavelength calibration is consistent and can be used to estimate Earth Lambertian albedo.
311 The wavelength dependence of the Earth's albedo peaks at 340 nm and decreases until
312 680 nm after which it increases slowly with wavelength. EPIC observed albedos for 551,
313 680, and 780 nm in March, June, and September show an increase when Africa is in view,
314 but a decrease for the blue 443 nm and UV channels. Earth's albedo is maximum in

https://doi.org/10.5194/egusphere-2026-1631
Preprint. Discussion started: 18 May 2026

December with all wavelength channels showing an increase at around 15:00 GMT for Earth images centered at a longitude of 45° west.

https://doi.org/10.5194/egusphere-2026-1631
Preprint. Discussion started: 18 May 2026

References

Akima, H., A New Method of Interpolation and Smooth Curve Fitting Based on Local Procedures, JACM, 589 – 602, https://doi.org/10.1145/321607.321609, 1970

Barkstrom, B. R., The Earth Radiation Budget Experiment (ERBE). *Bulletin of the American Meteorological Society, 65*(11), 1170–1185, 1984.

Cede, A., L.-K. Huang, G. McCauley, J. R. Herman, K. Blank, M. Kowalewski, and A. Marshak, Raw EPIC Data Calibration, Front. Rem. Sens., 2, doi: 10.3389/frsen.2021.702275, 2021.

Cede A., R. Rajagopalan, Y. Yu, A. Marshak, J. Herman, L. K. Huang, K. Blank, A. Smith, and S. Lorentz, 2025. EPIC and NISTAR radiometric stability assessment using ERA5 reanalysis data. Frontiers in Remote Sens., https://doi.org/10.3389/frsen.2025.1646764, 2025.

Cleveland, W.S., and Devlin, S.J., Locally Weighted Regression: An Approach to Regression Analysis by Local Fitting. Journal of the American Statistical Association, 83(403), 596-610. https://doi.org/10.1080/01621459.1988.10478639, 1988.

Csiszar, I., & Gutman, G., Mapping global land surface albedo from NOAA AVHRR. *Remote Sensing of Environment, 70*(3), 337–348, 1999.

Gettelman, A., Christensen, M. W., Diamond, M. S., Gryspeerdt, E., Manshausen, P., Stier, P., D. Watson-Parris, M. Yang , M. Yoshioka , and T. Yuan, Has reducing ship emissions brought forward global warming? Geophysical Research Letters, 51, e2024GL109077. https://doi. org/10.1029/2024GL109077, 2024.

Goessling, Helge F., Thomas Rackow, Thomas Jung, Recent global temperature surge intensified by record-low planetary albedo, Science, 387, 1-6, https://doi.org/10.1126/science.adq7280, 2025

Goode, P. R., Qiu, J., Yurchyshyn, V., Hickey, J., Chu, M.-C., Kolbe, E., Brown, C. T., & Koonin, S. E., Earthshine observations of the Earth's reflectance. *Geophysical Research Letters, 28*(9), 1671–1674, 2001.

Goode, P. R., Pallé, E., Shoumko, A.,Shoumko, S., Montañes-Rodriguez,P., & Koonin, S. E., Earth's albedo 1998–2017 as measured from earthshine. Geophysical Research Letters, 48, e2021GL094888. https://doi.org/10.1029/2021GL094888, 2021.

Gottwald, M., R. Hoogeveen, C. Chlebek, H. Bovensmann, J. Carpay, G. Lichtenberg, E. Krieg, P. Lutzow-Wentzky, and T. Watts (2011a), SCIAMACHY—Exploring the Earth's Changing Atmosphere, chap. 3, pp. 29–46, Springer, New York.

https://doi.org/10.5194/egusphere-2026-1631
Preprint. Discussion started: 18 May 2026

Harrison, E. F., Minnis, P., Barkstrom, B. R., Ramanathan, V., Cess, R. D., & Gibson, G. G., Seasonal variation of cloud radiative forcing derived from the Earth Radiation Budget Experiment. *Journal of Geophysical Research, 95*(D11), 18687–18703, 1980.

He, T., Liang, S., Wang, D., Shi, Q., & Goulden, M. L. (2014). Estimation of high-resolution land surface shortwave albedo from AVHRR data. *Journal of Geophysical Research: Atmospheres, 119*(23), 13,245–13,263, 2014.

Herman J. and Blank K., Fully illuminated Jupiter disk albedo and limb darkening observed by DSCOVR-EPIC from the Earth–Sun Lagrange-1 orbit. Front. Remote Sens. 6:1685883. doi: 10.3389/frsen.2025.1685883, 2025.

Jones A., Noll S., Kausch W., Szyszka C. and Kimeswenger S., An Advanced Scattered Moonlight Model for Cerro Paranal *A&A* **560** A91, DOI: 10.1051/0004-6361/201322433, 2013.

Karkoschka, E., Spectrophotometry of the Jovian Planets and Titan at 300 to 1000-nm wavelength: The methane spectrum, Icarus, 111, 174–192, https://doi.org/10.1006/icar.1994.1139, 1994.

Karkoschka, E., Methane, Ammonia, and Temperature Measurements of the Jovian Planets and Titan from CCD–Spectrophotometry, ICARUS 133, 134–146, https://doi.org/10.1006/icar.1998.5913, 1998.

Liu, J., Schaaf, C. B., Strahler, A. H., Jiao, Z., Shuai, Y., Zhang, Q., Roman, M., Augustine, J. A., & Hollinger, D. Y., Validation of MODIS albedo product (MCD43) over grassland, cropland, and forest. *Journal of Geophysical Research, 114*, D01106, 2009.

Loeb, N. G., Wielicki, B. A., Doelling, D. R., Smith, G. L., Keyes, D. F., Kato, S., Manalo-Smith, N., & Wong, T., Toward optimal closure of the Earth's top-of-atmosphere radiation budget. *Journal of Climate, 22*(3), 748–766, 2009.

Lucht, W., Andrew H. Hyman, Alan H. Strahler, Mike J. Barnsley, Paul Hobson, Jan-Peter Muller, A Comparison of Satellite-Derived Spectral Albedos to Ground-Based Broadband Albedo Measurements Modeled to Satellite Spatial Scale for a Semidesert Landscape, Remote Sensing of Environment,74, 85-98, https://doi.org/10.1016/S0034-4257(00)00125-5, 2000.

Mace, G. G., Benson, S., Gombert, P., and Smallwood, T.: Impact on cloud properties of reduced-sulphur shipping fuel in the Eastern North Atlantic, Atmos. Chem. Phys., 26, 1041–1051, https://doi.org/10.5194/acp-26-1041-2026, 2026.

https://doi.org/10.5194/egusphere-2026-1631
Preprint. Discussion started: 18 May 2026

Marshak, A., J. Herman, A. Szabo, K. Blank, A. Cede, S. Carn, I. Geogdzhaev, D. Huang, L.-K. Huang, Y. Knyazikhin, M. Kowalewski, N. Krotkov, A. Lyapustin, R. McPeters, K. Meyer, O. Torres and Y. Yang, Earth Observations from DSCOVR/EPIC Instrument., Bulletin Amer. Meteor. Soc. (BAMS), 9, 1829-1850, https://doi.org/10.1175/BAMS-D-17-0223.1, 2018.

Pallé, E., Goode, P. R., Montañés-Rodríguez, P., & Koonin, S. E., Changes in Earth's reflectance over the past two decades. *Science, 304*(5675), 1299–1301, 2004.

Penttilä A, Muinonen K, Ihalainen O, Uvarova E, Vuori M, Xu G, Näränen J, Wilkman O, Peltoniemi J, Gritsevich M, Järvinen H and Marshak A Temporal Variation of the Shortwave Spherical Albedo of the Earth. Front. Remote Sens. 3:790723. doi: 10.3389/frsen.2022.790723, 2022.

Qiu, J., Goode, P. R., Pallé, E., Shoumko, S., Shoumko, A., & Montañés-Rodríguez, P., Earth's albedo 1998–2017 from ground-based earthshine observations. *Nature Communications, 14*, 1234, 2023.

Robinson, Tyler, Inferring and Interpreting the Visual Geometric Albedo and Phase Function of Earth. 10.48550/arXiv.2507.22258, 2025.

Schaaf, C., F. Gao, A.H. Strahler, W. Lucht, X. Li, T. Tsang, N.C. Strugnell, X. Zhang, Y. Jin, J.-P. Muller, P. Lewis, M. Barnsley, P. Hobson, M. Disney, G. Roberts, M. Dunderdale, C. Doll, R. d'Entremont, B. Hu, S. Liang, J.L. Privette, D.P. RoyFirst operational BRDF, albedo, and nadir reflectance products from MODIS. *Remote Sensing of Environment, 83*(1–2), 135–148, 2002.

Stephens, G. L., D. O'Brien, P. J. Webster,P. Pilewski, S. Kato, and J.-l. Li, The albedo of Earth, Rev. Geophys., 53,141–163, doi:10.1002/2014RG000449, 2015.

Su, W., L. Liang, D. R. Doelling, P. Minnis, D. P. Duda, K. V. Khlopenkov, M.M. Thieman, N.G. Loeb, S. Kato, F. P. J. Valero, H. Wang, and F. G. Rose, Determining the shortwave radiative flux from Earth polychromatic imaging camera. J. Geophys. Res., 123, https://doi.org/10.1029/2018JD029390, 2018.

Taylor, V. R., & Stowe, L. L., Reflectance characteristics of Earth from satellite observations. *Journal of Geophysical Research, 89*(D4), 4987–4996, 1984.

Tosco, M., Calì Quaglia, F., Ciardini, V., Di Iorio, T., Iaccarino, A., Meloni, D., Muscari, G., Pace, G., Scarchilli, C., & di Sarra, A. G., Comparison of Broadband Surface Albedo from MODIS and Ground-Based Measurements at the Thule High Arctic Atmospheric

https://doi.org/10.5194/egusphere-2026-1631
Preprint. Discussion started: 18 May 2026

Observatory in Pituffik, Greenland, During 2016–2024. *Remote Sensing*, *17*(24), 3952. https://doi.org/10.3390/rs17243952, 2025.

Wang, D., S. Liang, T. He, Y. Yu, C. Schaaf,and Z. Wang, Estimating dailymean land surface albedo from MODIS data, J. Geophys. Res. Atmos., 120,4825–4841, doi:10.1002/2015JD023178, 2015.

Wielicki, B. A., Barkstrom, B. R., Harrison, E. F., Lee, R. B., Smith, G. L., & Cooper, J. E., Clouds and the Earth's Radiant Energy System (CERES): An Earth observing system experiment. *Bulletin of the American Meteorological Society, 77*(5), 853–868. https://doi.org/10.1175/1520-0477(1996)077<0853:CATERE>2.0.CO;2, 1996.

Wu, Jie, Enric Palle´, Huadong Guo, Yixing Ding, Long-term trends in albedo as seen from a lunar observatory, Advances in Space Research 72 2109-2117, DOI:10.1016/j.asr.2023.06.028, 2023.

Xu, X., J. Wang, Y. Wang, J. Zeng, O. Torres, J. Reid, S. Miller, J.V. Martins, and L. Remer, Detecting layer height of smoke aerosols over vegetated land and water surfaces via oxygen absorption bands: hourly results from EPIC/DSCOVR in deep space, Atmos. Meas. Tech., 12, 3269–3288, 2019, https://doi.org/10.5194/amt-12-3269-2019, 2019.

Yang, W., A. Marshak, T. Varnai and Y. Knyazikhin, EPIC spectral observations of the variability in Earth's global reflectance. Remote Sens., 10(2), 254, https://www.mdpi.com/2072-4292/10/2/254, 2018.

Yuan, Tianle, Hua Song, Robert Wood, Chenxi Wang, Lazaros Oreopoulos, Steven E. Platnick, Sophia von Hippel, Kerry Meyer, Siobhan Light, Eric Wilcox, Global reduction in ship-tracks from sulfur regulations for shipping fuel, Sci. Adv. 8, eabn7988, https://doi.org/10.1126/sciadv.abn7988 (2022)

Yin B., Q. Min, E. Morgan, Y. Yang, A. Marshak, and A. Davis, 2020. Cloud top pressure retrieval with DSCOVR-EPIC oxygen A and B bands observation. Atmos. Meas. Tech. 13, 1–18, https://doi.org/10.5194/amt-13-1-2020.

Data availability: The EPIC daily average counts/second are available from https://zenodo.org/records/19188194. The original EPIC data are available from The NASA Atmospheric Science Data Center (ASDC) https://asdc.larc.nasa.gov/project/DSCOVR. CERES data: https://ceres-tool.larc.nasa.gov/ord-tool/jsp/EBAFTOA421Selection.jsp

Funding: Funding for this research was obtained from the NASA DSCOVR-EPIC project

https://doi.org/10.5194/egusphere-2026-1631
Preprint. Discussion started: 18 May 2026

Acknowledgement: The authors thank the DSCOVR project for making the EPIC data available for analysis through the Langley Data Center.